

Experimental research on species compositions of nonequilibrium air plasma based on two-color Mach-Zehnder interferometry

Cite as: Phys. Plasmas **26**, 043514 (2019); <https://doi.org/10.1063/1.5090097>

Submitted: 24 January 2019 . Accepted: 01 April 2019 . Published Online: 19 April 2019

 Hao Sun,  Yi Wu, Zhixin Chen, Mingzhe Rong, Haodong Chang,  Fei Yang, and Chunping Niu



[View Online](#)



[Export Citation](#)



[CrossMark](#)

ARTICLES YOU MAY BE INTERESTED IN

[The effects of metal vapour on the fault arc in a closed, air-filled container](#)
Physics of Plasmas **26**, 043502 (2019); <https://doi.org/10.1063/1.5079304>

[The effect of adding an axial magnetic field on the expansion of a laser-produced plasma](#)
Physics of Plasmas **26**, 043515 (2019); <https://doi.org/10.1063/1.5089733>

[Investigation on the effects of the operating conditions on electron energy in the atmospheric-pressure helium plasma jet](#)
Physics of Plasmas **26**, 043506 (2019); <https://doi.org/10.1063/1.5087769>

AIP Advances

Fluids and Plasmas Collection

[READ NOW](#)

Experimental research on species compositions of nonequilibrium air plasma based on two-color Mach-Zehnder interferometry

Cite as: Phys. Plasmas **26**, 043514 (2019); doi: [10.1063/1.5090097](https://doi.org/10.1063/1.5090097)

Submitted: 24 January 2019 · Accepted: 1 April 2019 ·

Published Online: 19 April 2019



[View Online](#)



[Export Citation](#)



[CrossMark](#)

Hao Sun,¹ Yi Wu,^{1,a)} Zhixin Chen,² Mingzhe Rong,¹ Haodong Chang,¹ Fei Yang,¹ and Chunping Niu¹

AFFILIATIONS

¹State Key Laboratory of Electrical Insulation and Power Equipment, Xi'an Jiaotong University, Xi'an, Shaanxi 710049, People's Republic of China

²Electric Power Research Institute China Southern Power Grid Co., Ltd., Guangzhou 510080, Guangdong Province, China

^a)Author to whom correspondence should be addressed: wuyic51@mail.xjtu.edu.cn

ABSTRACT

An experimental method for the air plasma composition based on two-color Mach-Zehnder interferometry was established. By applying two laser beams with different wavelengths, the distributions of the temperature and nonequilibrium parameter were obtained. In the arc center, the energy exchange between the electrons and heavy particles is sufficient enough to make the plasma reach the equilibrium state. In this case, by comparing the electron density and neutral particle density derived from the interferograms, the calculated species compositions of air plasma under local thermal equilibrium were validated. Additionally, the distribution of the nonequilibrium parameter indicates that departure from the equilibrium occurs at the edge of the plasma and that the nonequilibrium area gradually expands during the arc decay phase. This trend is in good agreement with the two-temperature arc simulation, indicating the validity of the two-temperature arc model in many previous works.

Published under license by AIP Publishing. <https://doi.org/10.1063/1.5090097>

I. INTRODUCTION

Species compositions in thermal plasmas are the crucial parameters that determine the plasma behavior. Many researchers have investigated the species compositions of both equilibrium and nonequilibrium plasmas in recent years. However, due to the lack of experimental methods, the research on the species compositions of plasma mainly concentrates on the calculations. Although the calculation results are widely accepted and partially validated by comparing with the test results on the macroscopic plasma behaviors, like the voltage-current characteristics or the plasma motion, the species compositions have not yet been directly verified. Additionally, the verification of the species compositions by comparing the macroscopic parameters is not that convincible since the plasma behavior can be influenced by many other random factors, for example, the turbulence.

To find a better solution, various measurement methods based on spectral analysis have been applied to species composition measurements of plasma, such as the optical absorption spectrum (OAS) and the optical emission spectrum (OES), based on the absolute intensity method or the Stark broadening.^{1–10} This type of method obtains the electron number density and the electron temperature by analyzing the emission spectrum or the spectrum of the probe laser affected

by the plasma. However, the diagnosis of spectral analysis is mostly based on the local thermally equilibrium (LTE) assumption and cannot be applied to measure the nonequilibrium plasma. Additionally, the strict requirements of choosing spectral lines also limit this method to be applied in various kinds of plasmas. Another method of plasma measurement is the laser scattering including Thomson scattering and Rayleigh scattering. The procedure contains collecting scattered light by the plasma, analyzing the spectrum, and then obtaining related data including electron density, electron temperature, and heavy particle temperature. This method has high accuracy and does not depend on the LTE assumption. Therefore, it has been widely used in various occasions of plasma diagnosis.^{11,12}

Mach-Zehnder Interferometry is one of the methods that obtain the species compositions of plasma by measuring the refractive index and establishing the relationship between the refractive index and the number density of particles. The energy of the probe laser beam makes little influence on the plasma properties. Researchers can also improve the method to find out the temporal and spatial distribution of plasma properties by expanding the laser beam. By introducing the two laser beams with different wavelengths to form a plurality of interference fringes, the electron density and heavy particle density of the plasma

can be simultaneously obtained. This method is widely used in the diagnosis of various plasmas.^{13–23}

In this work, an experimental setup for the nonequilibrium compositions of air plasma based on two-color Mach-Zehnder interferometry was established. The temporal and spatial species compositions of air plasma were obtained and discussed. Finally, the test results were used to verify the calculation results of equilibrium and nonequilibrium species compositions.

II. TWO-COLOR MACH-ZEHNDER INTERFEROMETRY

A. Calculation of the plasma refractive index

By measuring the phase shift of the interferometric fringe after a probe laser beam goes through the plasma, from which the change of the refractive index of the plasma can be derived, Mach-Zehnder interferometry can be used to obtain the density and the species compositions of plasma. Therefore, it is necessary to establish the relationship between the refractive index of plasma and species compositions.

As a special electromagnetic wave, the laser beam can be altered by the electromagnetic field of the plasma, which is due to the influence of both the free electrons and the bound electrons of the heavy particles. The refractive index of the plasma η_p is determined by its permittivity ϵ_r ¹⁹

$$\eta_p = \sqrt{\epsilon_r} \quad (1)$$

and ϵ_r can be calculated by the dielectric polarization density \vec{P}_p as in the following equation:

$$\vec{P}_p = \epsilon_0(\epsilon_r - 1)\vec{E}, \quad (2)$$

where ϵ_0 and \vec{E} are the permittivity in vacuum and the electrical field of the laser excited by the harmonic wave, respectively. Thus, it is crucial to obtain the polarization density of plasma at a certain wavelength. As mentioned above, the polarization density is affected by both free electrons and bound electrons, which can be expressed by the sum of the polarization density by the free electrons \vec{P}_f and that by the bound electrons \vec{P}_b

$$\vec{P}_p = \vec{P}_f + \vec{P}_b. \quad (3)$$

\vec{P}_f can be derived from the ratio of the plasma frequency to the laser frequency as follows:

$$\vec{P}_f = -\epsilon_0 \frac{\omega_p^2}{\omega^2} \vec{E} = -\epsilon_0 \frac{r_e \lambda^2}{\pi} n_e \vec{E}, \quad (4)$$

$$\omega_p = \sqrt{n_e e^2 / m_e \epsilon_0}, \quad (5)$$

where ω_p and ω represent the plasma frequency and laser frequency, respectively; λ and n_e represent the wavelength of the laser beam and the electron number density in the plasma; and m_e and r_e are the electron mass and the classic electron radius, which can be given by

$$r_e = e^2 / 4\pi \epsilon_0 m_e c^2. \quad (6)$$

Assuming that the bound electrons in the heavy particles are the harmonic oscillators, their contributions to the polarization density can be expressed as

$$\vec{P}_b = \frac{e^2}{m_e} \left(n_i \sum_{k1} \frac{f_{k1}}{\omega_{0,k1}^2 - \omega^2} + n_n \sum_{k2} \frac{f_{k2}}{\omega_{0,k2}^2 - \omega^2} \right) \vec{E}, \quad (7)$$

where n_i and n_n are the number density of ions and neutral particles, respectively; f_k and ω_k are the oscillator strength and characteristic frequency of the k -th resonance level. Sangines and Sobral²² pointed out that the first term on the right of Eq. (7), meaning the contribution of ion, can be neglected. Then, \vec{P}_b can be simplified as²²

$$\vec{P}_b = \frac{e^2}{m_e} n_n \sum_{k2} \frac{f_{k2}}{\omega_{0,k2}^2 - \omega^2} \vec{E} = \epsilon_0 \frac{r_e}{\pi} n_n \sum_{k2} \frac{f_{k2} \lambda^2 \lambda_{0,k}^2}{\lambda^2 - \lambda_{0,k}^2} \vec{E}. \quad (8)$$

Therefore, the refractive index of plasma can be finally given by

$$\eta_p = \sqrt{1 - \frac{r_e \lambda^2}{\pi} n_e + \frac{r_e}{\pi} n_n \sum_k f_k \frac{\lambda^2 \lambda_{0,k}^2}{\lambda^2 - \lambda_{0,k}^2}}. \quad (9)$$

Furthermore, considering that the refractive index of plasma is much less than 1, Eq. (9) can be simplified as¹⁹

$$\eta_p \approx 1 - \frac{r_e \lambda^2}{2\pi} n_e + \frac{r_e}{2\pi} n_n \sum_k f_k \frac{\lambda^2 \lambda_{0,k}^2}{\lambda^2 - \lambda_{0,k}^2}, \quad (10)$$

where the last term of Eq. (10) represents the contribution of neutral particles to the refractive index of plasma, which is almost independent of the laser wavelength when the probe laser ranges from the visible light to the near-infrared light. Therefore, the last term can always be reduced to the Gladstone-Dale formula

$$\frac{r_e}{2\pi} n_n \sum_k f_k \frac{\lambda^2 \lambda_{0,k}^2}{\lambda^2 - \lambda_{0,k}^2} = \frac{\beta}{n_0} n_n, \quad (11)$$

where β is the Gladstone-Dale constant. This equation defines the refractive index of plasma as $1 + \beta$ when the number density of neutral particles equals the reference number density n_0 . The Gladstone-Dale constant of air at the standard temperature and pressure can be calculated by the Ciddor formula,²⁴ where $\beta \approx 2.7 \times 10^{-4}$ and $n_0 = 2.47 \times 10^{25} \text{ m}^{-3}$. Combining Eqs. (10) and (11), the refractive index of plasma can be written as follows, which is the basic equation in this work:

$$\eta_p = 1 - \frac{r_e \lambda^2}{2\pi} n_e + \frac{\beta}{n_0} n_n. \quad (12)$$

B. Species composition measurement based on Mach-Zehnder interferometry

As in Fig. 1, the Mach-Zehnder interferometer divides a laser beam into two coherent beams through a splitter. After passing the equal length of the optical path, the two beams are gathered at the second splitter and then form an interference image. The laser beam emitted from the light source first passes through a splitter and then two coherent laser beams are generated. One of the laser beams passes through the plasma, which is the probe laser; the other usually goes through a uniform medium, which is the reference laser. Two laser beams are reflected by a plane mirror and then combined by the second splitter to form the interference image, respectively. Since the probe laser beam goes through the plasma, the phase shift is formed in the interference image.

The relationship between the phase shift of interference fringes and the refractive index of the plasma can be computed by

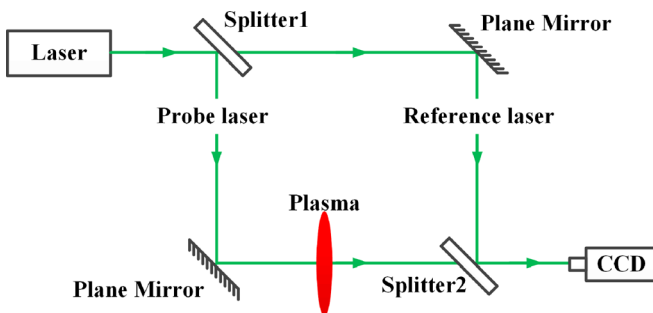


FIG. 1. Schematic view of the Mach-Zehnder interferometer.

$$\Delta\varphi(\lambda) = \frac{2\pi}{\lambda} \int_{s_1}^{s_2} (\eta_p(\lambda) - 1 - \beta) ds. \quad (13)$$

By using two laser beams with different wavelengths and combining Eqs. (12) and (13), the contributions of free electrons and those of bound electrons to the refractive index of the plasma can be distinguished. Thus, the number density of free electrons and neutral particles can be obtained by

$$\int_{s_1}^{s_2} n_e(s) ds = \frac{\lambda_1 \Delta\varphi_1 - \lambda_2 \Delta\varphi_2}{r_e(\lambda_2^2 - \lambda_1^2)}, \quad (14)$$

$$\int_{s_1}^{s_2} (n_n(s) - n_0) ds = \frac{n_0}{2\pi\beta} \frac{\lambda_2 \Delta\varphi_1 - \lambda_1 \Delta\varphi_2}{\lambda_2/\lambda_1 - \lambda_1/\lambda_2}. \quad (15)$$

In general, from the phase shifts of the two laser beams and Abel inversion,²⁵ the distributions of both the electrons and the heavy particles can be derived.

III. EXPERIMENTAL SETUP

The experimental setup for measuring the number density in the arc plasma based on two-color Mach-Zehnder interferometry is shown in Fig. 2. In this work, the two laser beams, which are 532 nm, MGL-III-532, Changchun New Industries Optoelectronics Technology Co., Ltd, and 635 nm, MDL-C-635, Changchun New Industries Optoelectronics Technology Co., Ltd, were used. Fringe images were recorded by a Phantom Miro M310 high speed camera. This measurement was carried out on the air plasma and the arc was ignited by separating the two electrodes. To avoid the influence of the electrode erosion, the material

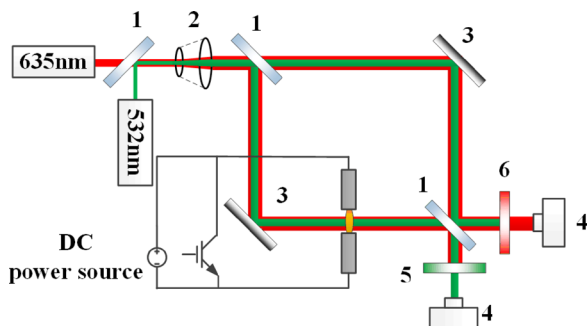


FIG. 2. Experimental scheme of two-color Mach-Zehnder interferometry: 1—splitter; 2—beam expander; 3—plane mirror; 4—high speed camera; 5—narrowband filter (532 nm); 6—narrowband filter (635 nm).

of the electrodes was chosen as graphite. The lower static contact was the cathode and the upper movable contact was the anode. Considering the stability and symmetry of the arc, the shape of the cathode was conical and the distance between the electrodes is no more than 5 mm. In addition, the arc plasma was at atmospheric pressure.

The DC source was used as the power supply, and the arc was turned on and off by controlling the IGBT (Insulated Gate Bipolar Transistor). The separation of the electrodes and the trigger of the high speed camera were controlled by DG535. At $t = 0$, the DC power supply was turned on together with the high speed camera. During this period, the IGBT was on and little current went through the electrodes as in Fig. 3. At $t = 10$ ms, the IGBT was off and the current was commuted to the arc branch. At the same time, the electrodes began to separate and the arc plasma was ignited and kept burning between the electrodes for 75 ms at a current of 60 A. After that, the IGBT was on again and the arc began to decay.

IV. MEASUREMENT AND ANALYSIS OF THE SPECIES COMPOSITIONS IN THE NONTHERMALLY EQUILIBRIUM AIR PLASMA

A. Analysis of interferogram of air plasma

In this section, the species compositions during the arc burning and arc decay were analyzed by Mach-Zehnder interferometry. Figure 4 shows Mach-Zehnder interference images of both the two laser beams when the air arc current is 60 A. The time sequence was consistent with that in Fig. 3. As mentioned in Sec. III, the arc was controlled very carefully, so the interference images in different tests are quite reproducible. Before 10 ms, the arc was not ignited, and the interference fringes remain in the initial state. After the arc ignition at $t = 10$ ms, the arc root was first located at the side of the movable contact and the arc keeps expanding with the electrode separation. On one hand, a large quantity of electrons was generated due to the ionization in the arc, which greatly reduced the refractive index of plasma, indicated by the second term in Eq. (12); on the other hand, the high temperature region has much lower number density of the neutral particles, which further decreased the refractive index. Therefore, the phase shift can be detected after the arc ignition. At $t = 20$ ms, the

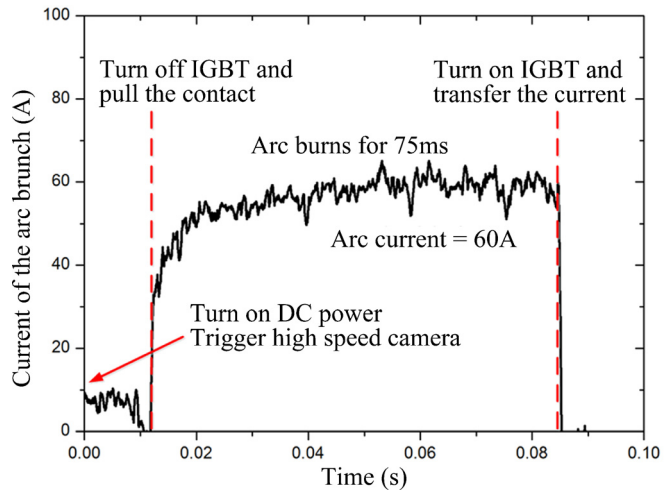


FIG. 3. Current waveform of the arc branch.

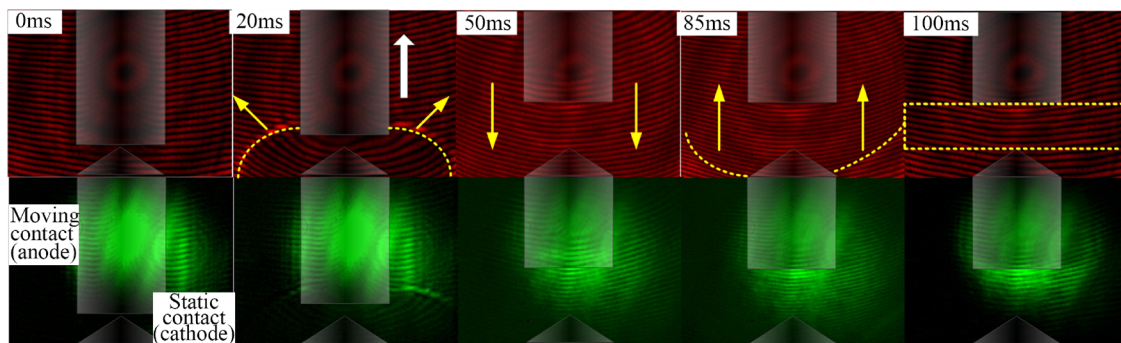


FIG. 4. Interference images versus time at the arc current of 60 A.

anode was still moving and the high temperature area has not expanded to the region above the anode yet. During this period, the interference fringes moved and the distortion of interference fringes can be detected at the edge of the high temperature area, which was marked by the yellow dashed lines. At $t = 50$ ms, the plasma region kept expanding and the interference fringes moved downward rapidly. After $t = 85$ ms, the IGBT was turned on and the arc began to decay. During the arc decay phase, the temperature decreased rapidly and the interference fringes moved up again. When the residual hot gas cooled down completely, the interference fringes tended to be stable and gradually recovered to the initial state at $t = 100$ ms as in Fig. 4. Additionally, in this test, no shock wave spreading in the radial direction was detected.

The results in Fig. 4 need to be further processed to obtain the refractive index and the species compositions of plasma. According to Singh *et al.*,²⁵ in this work to analyze the interference fringes, the IDEA software made by Hipp *et al.*²⁶ was adopted. As in Fig. 5, the results at $t = 85$ ms are taken as examples here. First, the image was transferred into the gray image, and the frequency of interference fringes is selected by Fourier transform to eliminate the noise. Then, the two-dimensional wrapped phase distribution with the amplitude between $-\pi$ and π was obtained, as in Fig. 5(a). Second, the phase was unwrapped using the algorithm of adjacent branch cutting, as in Fig. 5(b). Finally, subtracting the unwrapped phase distribution at $t = 85$ ms by the initial unwrapped phase at $t = 0$, the phase shift distribution was obtained, as in Fig. 5(c).

Figure 6 shows the phase shift of the 635 nm laser varying with time. Before $t = 10$ ms, no shift can be observed since the arc was not ignited yet. After that, the phase shift of the interference fringes decreased rapidly near the electrodes due to the strong production of the free electron in the plasma. Since the shape of the cathode was conical, the arc near the cathode was more concentrated and thus the phase shift is higher. As the arc keeps burning, the temperature of the arc tends to increase. However, according to Dalton's law, the electron number density does not always increase with the temperature. Therefore, when the temperature reached a certain value, there was a slight increase in the phase shift at $t = 60$ ms. Additionally, with a smaller arc radius, the arc near the cathode was more concentrated and the peak temperature was higher. As a result, the inflection point of the curve appears earlier near the cathode. After $t = 85$ ms, the sudden increase in the phase shift was due to the rapid decrease in the temperature during the arc decay. Finally, the phase shift dropped to a very low value. Still, the temperature of residual hot gas was higher than room temperature, and the gas density was not uniform. Therefore, the phase shift periodically oscillated and gradually approached zero.

B. Species compositions of air plasma derived from the test

From the results in Fig. 5(c), the distributions of the number density can be derived based on the Abel inversion. This section gives the

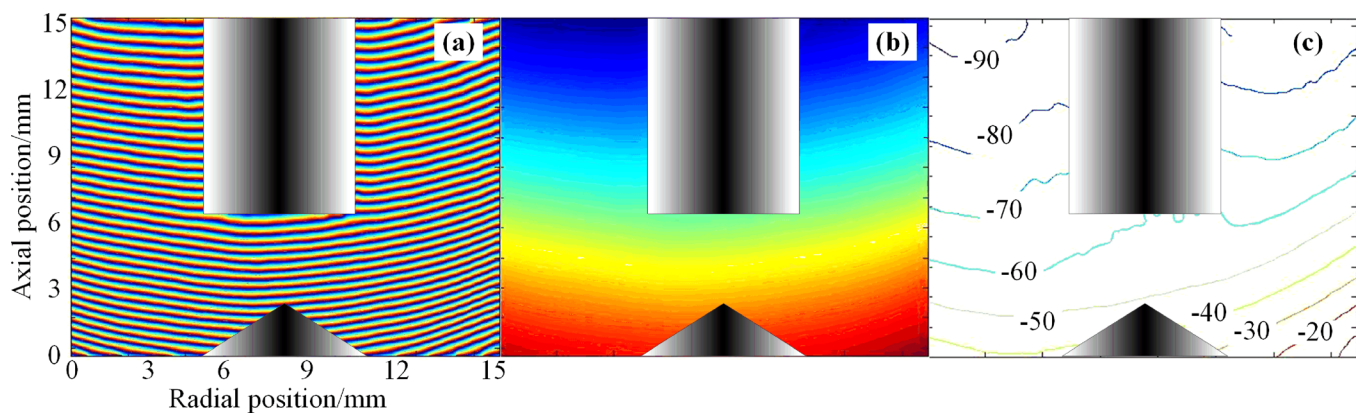


FIG. 5. Three steps for the phase analysis at $t = 85$ ms (arc current is 60 A): (a) wrapped phase distribution; (b) unwrapped phase distribution; (c) phase shift distribution.

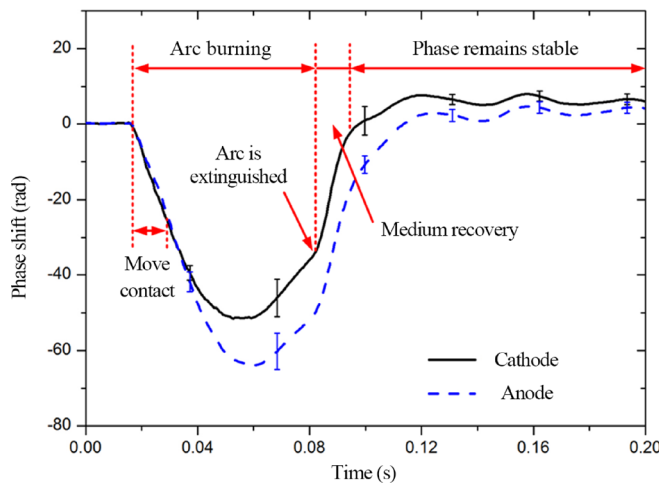


FIG. 6. Phase shift of the 635 nm laser near the cathode and anode.

results within 1.5 ms after the arc current reaches zero, and the concerned area is shown by the dotted rectangle in Fig. 4. From this section, $t=0$ refers to the moment the IGBT was on and the current dropped to zero. The distributions at $t=0$ clearly indicate that near the cathode, the arc was more concentrated and the peak temperature was higher. During the arc decay phase, due to the strong recombination and rapid cooling, it can be seen that the electron number density decreased fast. Additionally, the recovery of the phase shift occurred from the cathode to the anode, which was caused by the stronger cooling near the cathode. After 0.3 ms, the number density of free electrons near the cathode decreased from $2.1 \times 10^{23} \text{ m}^{-3}$ to $9.8 \times 10^{22} \text{ m}^{-3}$, and the number density of neutral particles increased from about 10^{22} m^{-3} to $3.7 \times 10^{23} \text{ m}^{-3}$, while near the anode, the number density of electrons decreased from $1.7 \times 10^{23} \text{ m}^{-3}$ to $7.9 \times 10^{22} \text{ m}^{-3}$. After 0.6 ms, the plasma near the cathode nearly fully recovered and the state of the medium transformed from conductive plasma into insulated residual hot gas. After 1.2 ms, the plasma near the anode decays rapidly. The

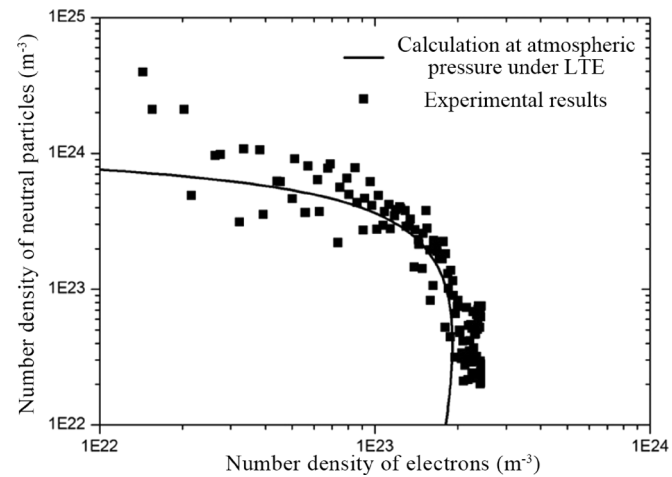


FIG. 7. Correspondence between electron number density and neutral particle number density obtained by experiment and comparison with the calculation under LTE.

electron number density was less than $1 \times 10^{22} \text{ m}^{-3}$, while the number density of neutral particles increased to $1 \times 10^{24} \text{ m}^{-3}$ or more. After 1.5 ms, generally the plasma in the electrode gap completely recovered, and the free electron density is lower than $1 \times 10^{20} \text{ m}^{-3}$. A high temperature region only exists near the anode center, and the neutral particle density was limited to about $1 \times 10^{24} \text{ m}^{-3}$.

C. Comparison of the species compositions between the test and calculation

Based on the number density of both the electron and neutral particle, the nonequilibrium parameter ($\theta = T_e/T_h$) can be calculated. Also in the arc center, usually the plasma can be considered to be equilibrium so that the comparison of the species compositions between the test and calculation can be made based on LTE, which is given in Fig. 7. It can be seen that the calculation agrees well with the test when

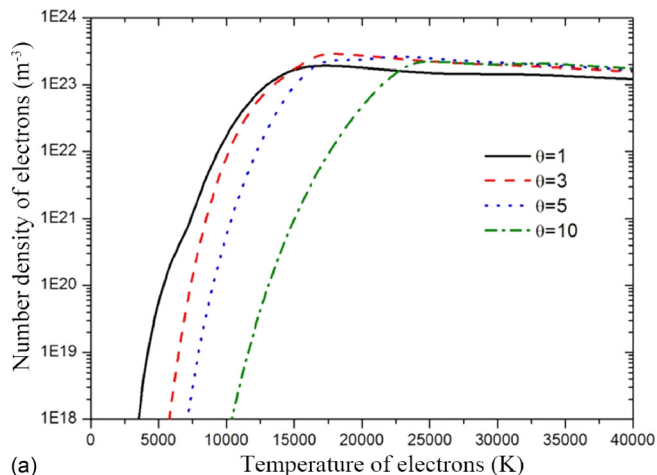
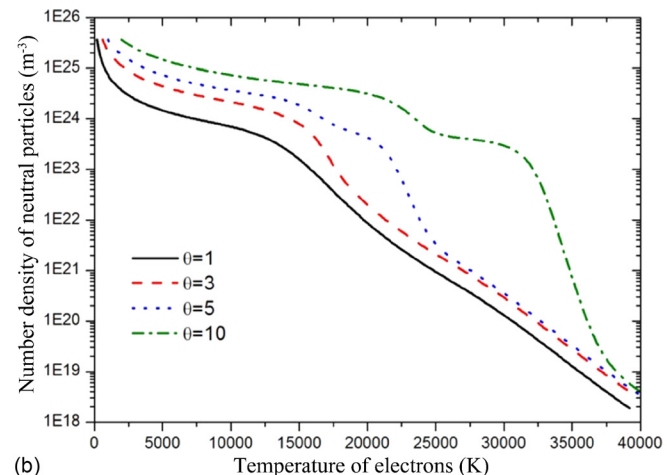


FIG. 8. Species compositions of air plasma versus electron temperature for different nonequilibrium parameters. (a) Number density of electrons and (b) number density of neutral particles.



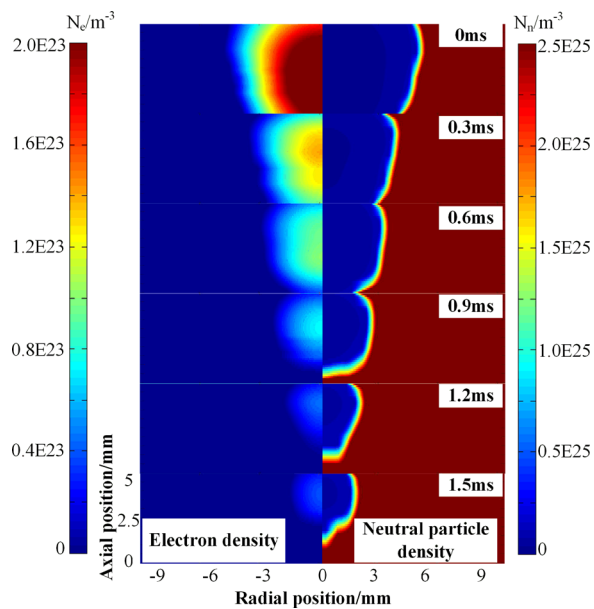


FIG. 9. The distributions of electron number density and heavy particle number density during the arc decay, derived from the area shown by the dotted rectangle in Fig. 4.

the electron number density is higher than 10^{23} m^{-3} . Therefore, in many previous works, the assumption of LTE in the arc center is proven to be reasonable here. However, when the electron number density is lower, departure from LTE can be clearly observed since the number density of neutral particles predicted by the calculation is lower than that predicted by the test as in Figs. 7 and 8. Additionally, the calculated electron number density in the arc center is slightly lower than that in the test. The reason is that the calculated results are based on the hypothesis that the pressure in the arc area is fixed as 1 atm, while in the real case in the arc center, the pressure could be higher, which is in correspondence with the work by Treilles *et al.*²⁸

Another importance of this work is that the distribution of the electron temperature and nonequilibrium parameter as in Fig. 10 can be further obtained by cross checking the test in Fig. 9 and the calculation in Fig. 8. At $t = 0$, in the arc center, the nonequilibrium parameter was around 1, implying the LTE in the arc center as mentioned above. However, at the edge of the arc, the energy exchange between the electrons and heavy particles is not sufficient, causing the departure from LTE. When the temperature further decreased to a very low value (below 5000 K), the nonequilibrium parameter decreased again. This is due to the fact that the number density of the heavy particles here is very high and the species compositions are dominated by T_h . This trend is in good agreement with the two-temperature arc simulation,^{27,28} indicating the validity of the two-temperature arc model in many previous works.

V. CONCLUSIONS

In Mach-Zehnder interferometry, the electron density and the neutral particle density make great contributions to the refractive index of air arc plasma and cause the phase shift of interference fringes. An experimental method for air plasma composition based on two-color

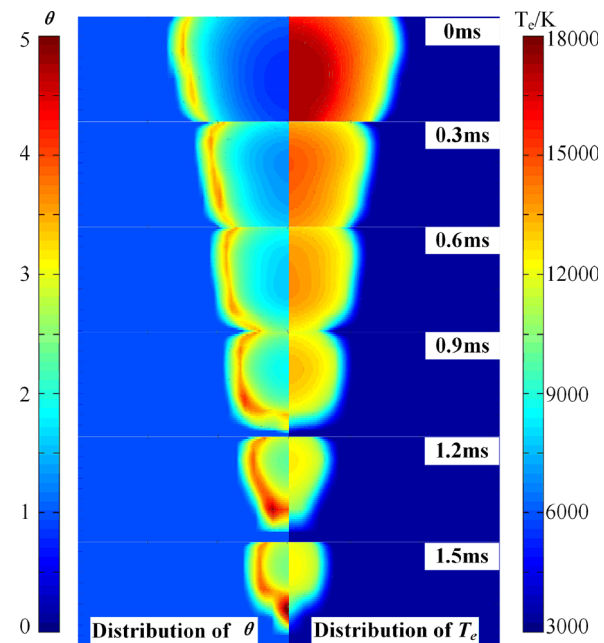


FIG. 10. Electron temperature and nonequilibrium distribution at different times during arc decay.

Mach-Zehnder interferometry was established. By using two laser beams with different wavelengths, the two dimensional distributions of temperature and nonequilibrium parameter were obtained by combining tests and calculations without the assumption of LTE. By processing the interferogram, the following conclusions can be made:

- (1) In the arc center, the energy exchange between the electrons and heavy particles is sufficient enough to make the plasma reach the equilibrium state. In this case, by comparing the electron density and neutral particle density, the calculated species compositions of air plasma in the arc center were validated.
- (2) The distribution of the nonequilibrium parameter indicates that departure from the equilibrium occurs at the edge of the plasma and that the nonequilibrium area gradually expands during the arc decay phase. This trend is in good agreement with the two-temperature arc simulation, indicating the validity of the two-temperature arc model in many previous works.

By applying this method to the plasmas of different gas media, this method can be further adopted in many occasions to obtain the detailed information of gas discharge.

ACKNOWLEDGMENTS

This work was supported by the National Key Basic Research Program of China (973 Program) 2015CB251001, National Natural Science Foundation of China under Grant Nos. 51577145, 51707144, and 51877165, and State Key Laboratory of Electrical Insulation and Power Equipment (EIPE19302).

REFERENCES

- ¹H. R. Griem and F. R. Scott, “Plasma spectroscopy,” *Am. J. Phys.* **33**, 864–865 (1961).

- ²H. J. Kunze, *Plasma Diagnostics*, Plasma physics (Springer, Berlin, Heidelberg, 2005), pp. 351–373.
- ³H. Griem, *Spectral Line Broadening by Plasmas* (Elsevier, 2012).
- ⁴D. R. Airey, P. H. Richards, and J. D. Swift, “Time-resolved radial temperature profiles for 10 kA SF₆ arcs,” *J. Phys. D: Appl. Phys.* **8**(16), 1982 (1975).
- ⁵G. R. Jones, W. Hu, and S. M. El-Kholi, “A spectroscopic investigation of electrode material entrained into the extinguishing arc of SF₆ circuit breaker,” *J. Phys. D: Appl. Phys.* **21**(9), 1414 (1988).
- ⁶R. Methling, S. Gorchakov, M. V. Lisnyak, S. Franke, A. Khakpour, S. A. Popov, and K. D. Weltmann, “Spectroscopic investigation of a Cu—Cr vacuum arc,” *IEEE Trans. Plasma Sci.* **43**(8), 2303–2309 (2015).
- ⁷D. T. Tuma, C. L. Chen, and D. K. Davies, “Erosion products from the cathode spot region of a copper vacuum arc,” *J. Appl. Phys.* **49**(7), 3821–3831 (1978).
- ⁸J. E. Jenkins, J. C. Sherman, R. Webster, and R. Holmes, “Measurement of the neutral vapour density decay following the extinction of a high-current vacuum arc between copper electrodes,” *J. Phys. D: Appl. Phys.* **8**(12), L139 (1975).
- ⁹D. Hong, G. Sandolache, J. M. Bauchire, F. Gentils, and C. Fleurier, “A new optical technique for investigations of low-voltage circuit breakers,” *IEEE Trans. Plasma Sci.* **33**(2), 976–981 (2005).
- ¹⁰B. Horvath and T. Lamara, “Time-resolved optical resonant absorption spectroscopy of Cr metallic vapor in air using a broadband LED light source,” *Plasma Sources Sci. Technol.* **22**(4), 045006 (2013).
- ¹¹K. Tomita, D. Gojima, K. Nagai, K. Uchino, R. Kamimae, Y. Tanaka, and T. Shinkai, “Thomson scattering diagnostics of decay processes of Ar/SF₆ gas-blast arcs confined by a nozzle,” *J. Phys. D: Appl. Phys.* **46**(38), 382001 (2013).
- ¹²S. C. Snyder, G. D. Lassahn, and L. D. Reynolds, “Direct evidence of departure from local thermodynamic equilibrium in a free-burning arc-discharge plasma,” *Phys. Rev. E* **48**(5), 4124 (1993).
- ¹³X. B. Zou, X. X. Wang, M. Han *et al.*, “Experimental study of implosion plasma physical characteristics in a small puff-gas z-pinch,” *AIP Conf. Proc.* **808**(1), 181–184 (2006).
- ¹⁴X. Zou, X. Wang, C. Luo *et al.*, “Measuring the evolution of electron density profile in a small gas-puff z-pinch,” *IEEE Trans. Fundam. Mater.* **124**(6), 515–518 (2010).
- ¹⁵O. Iwase, W. Süß, D. H. H. Hoffmann, M. Roth, C. Stöckl, M. Geissel, and R. Bock, “Laser-produced plasma diagnostics by a combination of Schlieren method and Mach-Zehnder interferometry,” *Phys. Scr.* **58**(6), 634 (1998).
- ¹⁶Y. Tao, M. S. Tillack, S. S. Harilal, K. L. Sequoia, B. O’Shay, and F. Najmabadi, “Effect of shockwave-induced density jump on laser plasma interactions in low-pressure ambient air,” *J. Phys. D: Appl. Phys.* **39**(18), 4027 (2006).
- ¹⁷P. Hough, T. J. Kelly, C. Fallon, C. McLoughlin, P. Hayden, E. T. Kennedy, and J. T. Costello, “Enhanced shock wave detection sensitivity for laser-produced plasmas in low pressure ambient gases using interferometry,” *Meas. Sci. Technol.* **23**(12), 125204 (2012).
- ¹⁸H. Zhang, J. Lu, Z. Shen, and X. Ni, “Investigation of 1.06 μm laser induced plasma in air using optical interferometry,” *Opt. Commun.* **282**(9), 1720–1723 (2009).
- ¹⁹G. Point, Y. Brelet, L. Arantchouk, J. Carbonnel, B. Prade, A. Mysyrowicz, and A. Houard, “Two-color interferometer for the study of laser filamentation triggered electric discharges in air,” *Rev. Sci. Instrum.* **85**(12), 123101 (2014).
- ²⁰K. Muraoka, M. Hamamoto, and M. Akazaki, “Studies of an impulse spark using two-wavelength interferometry,” *Jpn. J. Appl. Phys., Part 2* **19**(6), L293 (1980).
- ²¹A. J. Alcock and S. A. Ramsden, “Two wavelength interferometry of a laser-induced spark in air,” *Appl. Phys. Lett.* **8**(8), 187–188 (1966).
- ²²R. Sangines and H. Sobral, “Two-color interferometry and shadowgraphy characterization of an orthogonal double-pulse laser ablation,” *J. Appl. Phys.* **110**(3), 033301 (2011).
- ²³Z. Yang, J. Wu, W. Wei, X. Li, J. Han, S. Jia, and A. Qiu, “Laser-induced plasmas in air studied using two-color interferometry,” *Phys. Plasmas* **23**(8), 083523 (2016).
- ²⁴P. E. Ciddor and R. J. Hill, “Refractive index of air. 2. Group index,” *Appl. Opt.* **38**(9), 1663–1667 (1999).
- ²⁵R. P. Singh, S. L. Gupta, and R. K. Thareja, “Optical probe investigation of laser ablated carbon plasma plume in nitrogen ambient,” *Phys. Plasmas* **20**(12), 123509 (2013).
- ²⁶M. Hipp, J. Woitschläger, P. Reiterer, and T. Neger, “Digital evaluation of interferograms,” *Measurement* **36**(1), 53–66 (2004).
- ²⁷W. Wang, J. D. Yan, M. Rong, A. B. Murphy, and J. W. Spencer, “Theoretical investigation of the decay of an SF₆ gas-blast arc using a two-temperature hydrodynamic model,” *J. Phys. D: Appl. Phys.* **46**(6), 065203 (2013).
- ²⁸J. P. Trellis, J. V. R. Heberlein, and E. Pfender, “Non-equilibrium modelling of arc plasma torches,” *J. Phys. D: Appl. Phys.* **40**(19), 5937 (2007).